Journal of
Ceramic Science
and Technology

J. Ceram. Sci. Technol., **08** [3] 399-410 (2017)
DOI: 10.4416/JCST2017-00051
available online at: http://www.ceramic-science.com
© 2017 Göller Verlag

Boronhydride-Geopolymer Composites

C.H. Rüscher*

Institut für Mineralogie, Leibniz Universität Hannover, Callinstr. 3, 30167 D-Hannover, Germany
received June 21, 2017; received in revised form August 8, 2017; accepted August 24, 2017

Abstract

Sodium tetrahydroborate ($NaBH_4$ = SB) and ammonia-borane (NH_3BH_3 = AB) were dissolved in sodium aluminate and silicate solutions. Bringing them together caused immediate gel formation and recrystallization of SB and AB during drying. The gel forms geopolymer (G) type units, which enclose and protect the SB and AB crystals inside. SB-G composites are stable over a long time without any loss in SB. An optimized SB-G releases about 1820 L hydrogen per kg, i.e. containing an equivalent of about 80 % of pure SB (2270 L/kg) obtained by means of acidic titration. SB and SB-G remain stable up to 400 °C in vacuum and under inert gas conditions (He, Ar, N_2). In air, a reaction starts at about 240 °C, leading to a complete transformation to $NaBO_2$ above about 320 °C. For SB-G, this reaction is retarded by 50 °C. In the case of AB-G, IR-absorption spectra indicate that the geopolymer matrix consists of mainly sialate units (Si-O-Al-O). Heating experiments at temperatures of 120, 150 and 300 °C show the formation of polyaminoboranes (PAB) and polyiminoboranes (PIB). The underlying reactions could be related to hydrogen release in two exothermic peaks observed at around 122 °C and 160 °C. There are strong indications that DADB, the diammoniate of diborane, $(NH_3BH_2)[BH]_4$, forms prior to hydrogen release in the first step.

Keywords: Hydrogen storage, AB-geopolymer, SB-geopolymer

I. Introduction

Boron hydrides have received attention as hydrogen storage materials thanks to their remarkable gravimetric and volumetric hydrogen contents. However, there are significant problems concerning their application, e.g. unfavorable hydrogen releasing temperature, slow releasing rates, formation of borazine and other volatile gases, instabilities when exposed to moisture, leading to uncontrollable hydrogen depletion, lack of reversibility. This has necessitated the development of some scaffold scenarios for better handling. For example, in the case of ammonia-borane (NH_3BH_3 = AB), this could be loaded into mesoporous graphitic carbon nitride (MGCN) via a solution-impregnation route [1], infiltrated into mesoporous silica SBA-15 [2] and silica hollow nanospheres [3]. ZIF-8, a zeolite-type MOF (metal organic framework), could be used to immobilize Ni-nanoparticles, obtaining a highly effective catalyst for hydrogen generation from hydrolysis of AB, too [4]. Mesoporous silica, MCM-41, was investigated as an alternative means to stabilize or destabilize infiltrated ammonium borohydride, NH_4BH_4 (= ABH_2) [5].

The above-mentioned method of impregnation or infiltration procedure could be traced back to Barrer's idea [6] for loading zeolites like A, X, Y with boron salts like $NaBH_4$ (= SB) or $Al(BH_4)_3$. However, this idea could never be realized. Another method to encapsulate the BH_4-anion in sodalite cages was discovered based on a direct hydrothermal synthesis technique [7–10]. This method only proved successful for the sodalite (SOD) itself [10]. Hydrogen could be thermally released stepwise [10, 11] in the reaction of the BH_4-anion protected and separated in the sodalite cage with water molecules provided by a matrix that glues the nanocrystals together into larger units. However, the $NaBH_4$-sodalite ($Na_8Si_6Al_6O_{24}(BH_4)_2$) can contain a maximum of only 0.5 % SB by weight. For applications as hydrogen storage systems, much higher densities of BH_4-anions are required. Alkaline solutions containing a maximum of 30 wt% SB are currently used in fuel cell applications [12]. SB contains 10 wt% hydrogen, respectively 1.2 L of hydrogen per gram (density 1.07 g/cm³). The release of hydrogen is doubled in the reaction with water. It is interesting to note that the new SB-geopolymer (SB-G) composite material could release up to 1.8 L H_2 per gram [13]. This means that high hydrogen contents could be handled easily in geopolymer-type materials. It has also been reported that AB could be enclosed in a similar way in a geopolymer matrix [14].

It is the purpose of the present contribution to briefly summarize the main results obtained for SB and AB enclosed in geopolymers.

II. Experimental

Solutions of sodium-aluminate ($NaAlO_2$, Riedel de Haen 13404), solution I and of sodium-silicate (Na_2SiO_3, Fluka 307815), solution II, were prepared by dissolving each in 1.5 mL of deionized water at a temperature of not more than 60 °C. The amounts of each material used to prepare the solution are given in Table 1. Solubility experiments showed that a maximum of 850 mg of SB could be dissolved in appropriate solutions I and II, revealing clear

* Corresponding author:
c.ruescher@mineralogie.uni-hannover.de

liquids during stirring. Always half of the amount of SB (Merck, 806373) given in Table 1 was added to solution I and II. Mixing these solutions causes immediate gel precipitation. Solution II was added drop by drop to solution I. With the first drop added, gel formation was initiated. The obtained gels were stirred until they appeared homogenized. The gels were then dried at the temperatures and times given in Table 1. Also given in Table 1 are the amounts of H_2 released and the effectively enclosed SB in the geopolymer related to these, as described below.

The preparation of AB-containing aluminosilicate gels follows closely the route described for SB-G composites. Specifically, 245 mg AB (Aldrich, 287717, technical grade 90 %) was added into a sodium-aluminate solution (250 mg $NaAlO_2$ in 1.5 mL distilled H_2O) and the same amount into a sodium-silicate solution (310 mg Na_2SiO_3, Fluka 307815, in 1.5 mL distilled H_2O). Clear solutions were obtained by stirring within some minutes. Mixing of these solutions causes immediate gel precipitation. The gel was dried at 80 °C in air for 3 h and a white powder was obtained.

XRD was performed with a Bruker D8 powder diffractometer (CuKα radiation, 2 theta range 5° to 80°, step width of 0.02° and measuring time of 2 sec/step). The obtained data were evaluated with STOE WinXpow and Bruker TOPAS software. Thermogravimetric/differential thermoanalyses (TG/DTA) were conducted using Setaram 1650 equipment. Heating/cooling runs were carried out under He or technical air (N_2/O_2 80/20) flowing conditions (20 mL/minute) with a rate of 5 K per minute. FTIR spectra (Bruker Vertex 80v) were captured systematically using the KBr method on the as-received samples, after the TG experiment.

Table 1: Drying method, amount of solids used, SB/solid ratio (R) and molar ratio Si/Al of series of samples as denoted (S2-S8, S9-S13) and for a sample using "optimized conditions", S1. Also given are amounts of H_2 released and SB effectively enclosed in the geopolymer.

Sample name	Drying method	$NaBH_4$ (mg)	$NaSiO_3$ (mg)	$NaAlO_2$ (mg)	SB/solid (R)	Molar Si/Al	H_2 (L/g)	% SB_{eff} enclosed
Gel_80_0,5	80 °C, 4h	497	215	290	0.5	0.50	1.10	86.6
Gel_80_1	80 °C, 4h	500	302	200	0.5	1.00	1.19	93.2
Gel_80_1,5	80 °C, 4h	503	344	154	0.5	1.50	1.18	92.7
Gel_80_2	80 °C, 4h	494	380	128	0.5	2.00	1.26	99.2
S1	85 °C, 3h	1704	449	111	0.75	2.72	1.82	95.2
S2	110 °C, 2h	560	160	400	0.5	0.27	1.06	83.5
S3	110 °C, 2h	600	200	400	0.5	0.34	1.07	83.7
S4	110 °C, 2h	500	200	300	0.5	0.45	1.12	88.3
S5	110 °C, 2h	600	300	300	0.5	0.67	1.11	87.4
S6	110 °C, 2h	500	300	200	0.5	1.01	1.10	86.6
S7	110 °C, 2h	400	300	100	0.5	2.01	1.19	93.2
S8	110 °C, 2h	750	600	150	0.5	2.69	1.21	95.2
S9	110 °C, 2h	200	250	310	0.26	0.83	0.41	61.3
S10	110 °C, 2h	500	250	310	0.47	0.83	0.93	77.7
S11	110 °C, 2h	800	250	310	0.59	0.83	1.23	81.6
S12	110 °C, 2h	1200	250	310	0.68	0.83	1.50	86.4
S13	110 °C, 2h	1700	250	310	0.75	0.83	1.63	85.4
S14	60 °C, 6h	500	250	310	0.47	0.83	0.96	80.5
S15	80 °C, 4h	500	250	310	0.47	0.83	1.08	90.1
S16	95 °C, 3h	500	250	310	0.47	0.83	1.12	93.9
S17	110 °C, 2h	500	250	310	0.47	0.83	0.94	78.4
S18	60 °C, 6h	800	250	310	0.59	0.83	1.15	76.7
S19	80 °C, 4h	800	250	310	0.59	0.83	1.45	96.7
S20	95 °C, 3h	800	250	310	0.59	0.83	1.41	93.7
S21	110 °C, 2h	800	250	310	0.59	0.83	1.23	81.6

The hydrogen content of the geopolymer composites was measured using the same procedure as described earlier [10, 11]. For example, for complete release of the hydrogen from the SB-G composite, the diluted acid (1M HCl) has to be added in a surplus. The added volume of acid was varied between 5 and 8 mL and was subtracted afterwards from the shown volume at the gas syringe (Fig. 1) so as to register only the amount of released gas. The diluted acid was injected with an injection needle through the plug. The apparatus remains gastight. For every sample, different masses in a range between 10 and 80 mg were investigated. With linear regression, an amount of released hydrogen per 100 mg sample was calculated. Owing to the vertical assembly of the gas syringe, the additional weight of the plunger had to be considered. Its influence on the measured volumes was calculated and added to the results. Corrections contain the influence of the volume of the added acid to the measured gas volume in the gas syringe. Uncertainties are related to the reading error, which show some scatter of data minimized by the linear regression, using the *RGP-function* of *Microsoft Excel*. The released gas volume contains hydrogen, which was checked based on the hydrogen-oxygen reaction. Additionally, the released gas was checked with a gas detector, showing the released gas contains no CO_2 (detection limit < 1000 ppm). The data were used to estimate the amount of SB contained in the geopolymer with two assumptions: i. the SB is reacted completely, and ii. four moles of hydrogen (H_2) are released per mol SB, taking the additional contribution of H_2O into account. Accordingly, the percentage of mass of SB used during synthesis is compared to the apparent percentage of mass calculated from the obtained amount of hydrogen.

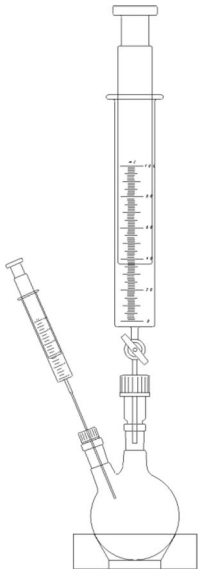

Fig. 1: Glass ware apparatus for gas release (100 mL bulb).

III. Results and Discussion

(1) SB-G composites

(a) *XRD*

The X-ray powder patterns of series of samples obtained by drying at 80 °C are shown in Fig. 2a – d. The samples show a very broad peak in the range 20 to 40 ° 2-theta with maxima around 28 – 32 ° 2-theta, which is related mainly to the formation of short-range-ordered or pairs of siloxo and sialate units. The broader diffraction peaks that appear in the pattern of Si/Al ratio 1, 1.5 and 2 are related to nanocrystalline or not well crystallized sodalites (marked by A in Fig. 2). In all cases, the presence of SB crystals can be identified, as marked by B (peaks consistent with ICSD 165707). Further peaks could be identified as sodium carbonate (C) and the sample holder (P). Some additional lines (B*) were observed in a few cases (Fig. 2b, c), which could be identified as $NaBH_4{\cdot}H_2O$ (ICSD 419041, compare also [15]). The X-ray pattern shows close similarities to those previously reported where a series of samples of Si/Al ratio of 0.8 and SB/solid ratio of R = 0.75 has been investigated [10, 11]. There it was observed that immediately after gel formation a broad hump occurs similar to that observed in Fig. 2a, without, however, any indication of more sharper diffraction peaks. Crystallization of sodalites occurred after 0.5 h drying at 110 °C and recrystallization of SB could be obtained in the pattern of the 1-h-dried sample, which significantly increases on further drying.

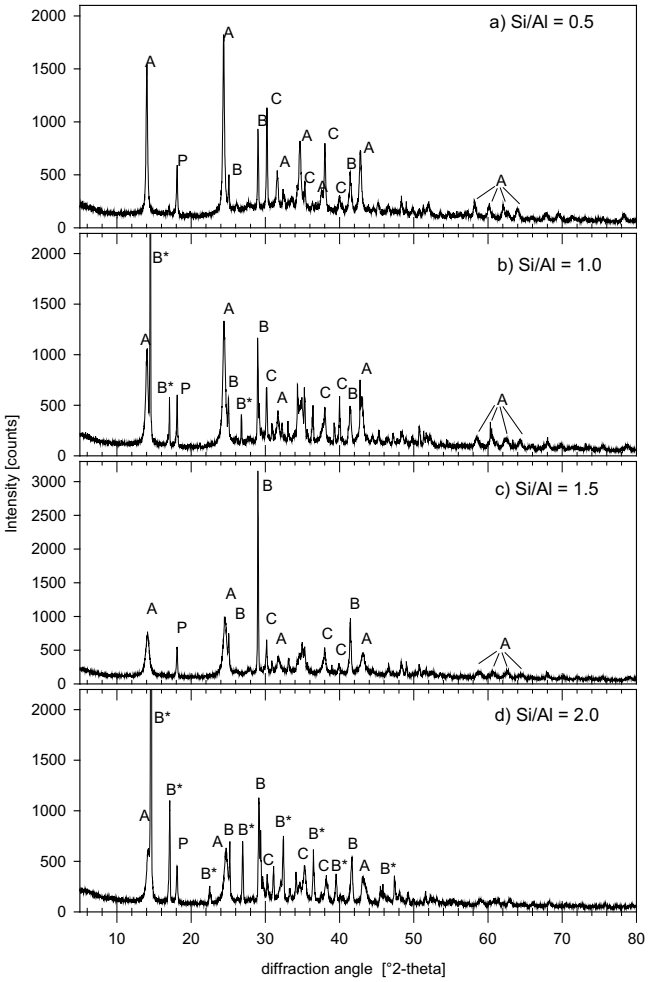

Fig. 2: X-ray powder pattern of as-received 80 °C dried samples (Gel_80, Table 1). Marked: A = sodalite, B = SB, B* = $NaBH_4{\cdot}2H_2O$, C = carbonate, P = sample holder. (modified from [13]).

The diffraction patterns of series of samples for drying at 110 °C for 1 and 2 h showed in all cases very close similarity

to the pattern also obtained for samples dried at 80 °C for 4 h. For the 110 °C-dried samples, the broad geopolymer-related peak appeared to be reduced in intensity in respect of the better crystallized sodalite contribution.

(b) ***IR absorption***

The series of samples were further investigated by means of infrared absorption of as-received samples as well as samples after 3 and 9 months of ageing in closed glass bottles. No significant alteration as a result of the longer holding time could be observed from a comparison of the spectra of the as-received samples (Fig. 3a) and 9-month-aged samples (Fig. 3b). The typical appearance is first of all a clear indication of SB in all cases. SB shows characteristic peaks with maxima at 1126, 2224, 2286 and 2386 (all given in cm^{-1}) at the same positions also observed for the pure salt, using the KBr method. The suggested tetrahedral BH_4-unit, which ideally allows only two IR active vibrations (ν_4, ν_3), shows two additional peaks (e.g. [15]). One has been explained based on the Fermi Resonance effect according to $2\nu_4$ (1128) ≈ ν_3,which leads to a splitting and sharing of intensity resulting into the two peaks at 2224 and 2284. The other one is explained based on a combination effect $\nu_4 + \nu_2$ (ν_2 = Raman active mode observed at 1273), leading to the peak at 2386 cm^{-1}.

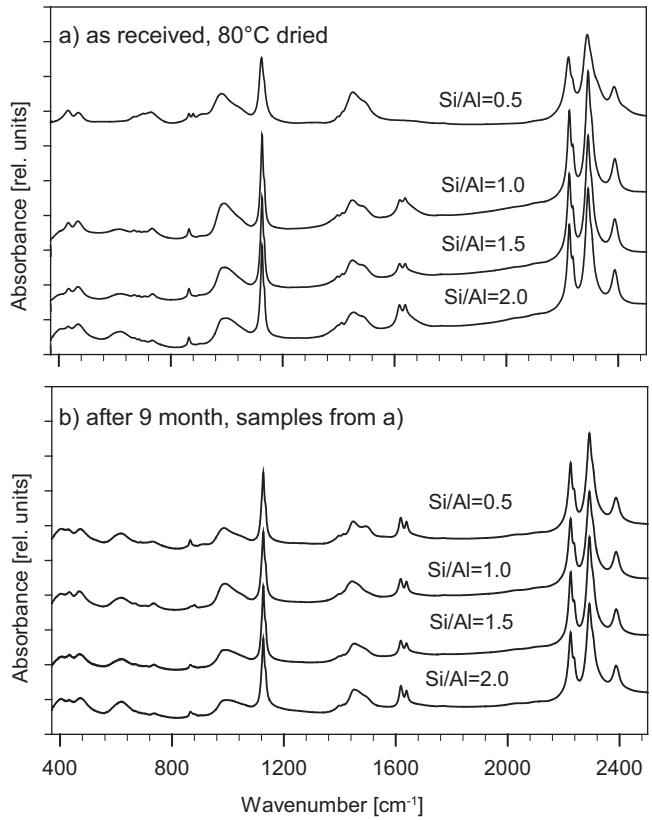

Fig. 3: FTIR absorption spectra of as-received samples a) gel_80 as received b) after 9 months.

The presence of the geopolymer in the spectra of $NaBH_4$-geopolymer composite has been demonstrated earlier [10,11] to be attributable to broad peaks with maxima around 1000, 700 and 450 cm^{-1} (compare also below, Fig. 10). In the spectra shown in Fig. 3, the geopolymer contribution is superimposed by other features. These are related to sodalite framework vibrations, contributions of sodium carbonate and $NaBr{\cdot}2H_2O$. The effect of various contributions and different Si/Al ratio is depicted more clearly in Fig. 4, showing a spectrum of $NaBH_4$-sodalite and two spectra of the 80 °C series, namely the Si/Al = 0.5 and 2 as-received samples using a $NaBH_4$-to-solid ratio R = 0.5. Another spectrum shown is that of the sample prepared using Si/Al = 2.75, R = 0.75 and dried at 85 °C, which contained the highest amount of hydrogen released here (see below).

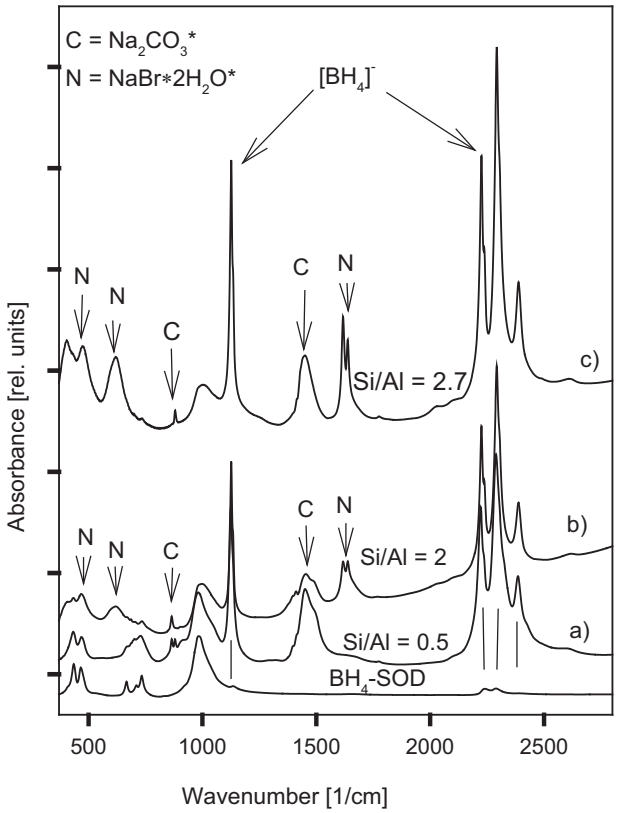

Fig. 4: FTIR absorption spectra of Gel_80_0,5 a), Gel_80_2 b), S1 d) (compare Table 1), and BH_4-sodalite. (*mark additional phases from contamination as explained in the text).

The absorption characteristics of SB can be deduced as marked and described above. In the spectra, the contribution of $NaCO_3$ is marked, too, this is due to the carbonation effect of the alkaline solutions handled under open conditions. The characteristic peak positions of $NaBr{\cdot}2H_2O$ are also marked. These contributions can be seen in all spectra in Fig. 3 but one, namely that of 80 °C as-received for Si/Al = 0.5, as also shown in Fig. 4. The formation of this phase is related to the presence of water molecules and an exchange between Na and K ions from the sample and the matrix during pressing of the pellets. The contribution of sodalite framework vibration can be seen to a more or lesser extent in all spectra shown in Fig. 3. For comparison, $NaBH_4$-sodalite shows the strongest framework vibrations with a maximum at (all in cm^{-1}) 987, the triplicate characteristic 733, 703, 667 and double peak with maxima at 436, 471, Fig. 4. The $NaBH_4$-sodalite spectrum chosen for better comparison also shows the BH_4-group-related vibrations. It can be seen that their intensities are small relative to the framework contribution and would not contribute significantly

to the BH_4-absorption intensity observed for the composite. We rule out that the sodalite formed in the composite material is of the BH_4-sodalite type, but rather of the hydro-hydroxy sodalite type [10]. Although the main three broad peaks of the geopolymer contribution fall into the same range of strong sodalite phonons, a systematic change in geopolymer composition might be deduced using the main peak maximum in the density of states of asymmetric vibrations of $[SiO_4]$-units. There is a shift in the position of the peak maximum related to the Si/Al ratio given by the compositions of solution I and II as could be seen in the 80 °C-dried samples (Fig. 3, 4), which is verified in the series of samples dried at 110 °C, too (Fig. 5). In particular, the maximum is changed from 990 towards 1005 cm^{-1} when the Si/Al ratio of the mixed solutions I and II is increased from 1 to 2.7. This might indicate a relative increase in the contents of disiloxo units relative to sialate units in the geopolymer matrix. Similar trends are also observed in the IR-absorption spectra following the change in composition of zeolite X with Si/Al ratio between 1 and 1.5 to zeolite Y (X = 2.4) in the intermediate range of compositions [16]. This is interesting to note since similar structural units can be expected for both families of compounds. The spectra also show a peak of decreasing area with increasing Si/Al ratio at 960 cm^{-1}, which is attributed to Al-(OH)-vibrations of six-fold coordinated Al^{3+}. These species are absent for Si/Al ≥ 1, indicating an excess of Al not included in the geopolymer network for smaller Si/Al.

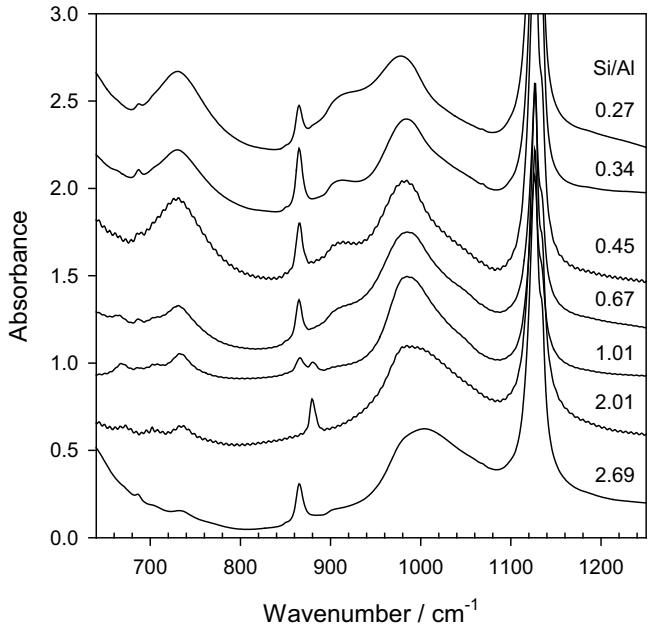

Fig. 5: Enlarged range of FTIR absorption spectra of as-received samples S2 to S8 (Table 1).

(c) ***Hydrogen content***

An approximately linear increase of the hydrogen released for a series of samples dried at 110 °C and using a fixed Si/Al ratio of 0.83 (S9 – S13, Table 1) could be observed with an increase in the amount of SB along the SB/solid ratio (Fig. 6a). The content obtained for the sample of lowest R constitutes about 45 mL H_2/100 mg sample. The linear increase in hydrogen released could well be extrapolated to the value obtained for SB, i.e. 2.26 L/g for R = 1. This value is below the expected ideal value of 2.4 L/g of SB which could be related to a systematic underestimate of the hydrogen contents in the glass ware apparatus. The highest value of hydrogen release along this series (S9 – S13) is 1.63 L/g, which is related to the solubility limit of SB in the appropriate aluminate and silicate solution used here. This value is close to the solubility of SB in water (5.5 g/L). The experiments indicate that the highest SB/solid ratio that can be reached is 0.75. At higher ratios, the SB cannot be dissolved completely, neither in the alumina-solution nor in the silica-solution. An increase of the water amount for the synthesis-solutions at constant SB/solid ratio to dissolve more SB causes problems during gel precipitation: With higher amounts of water, the gel precipitation time increases, which is responsible for an increase in the loss of SB and thus lower hydrogen contents. We also checked appropriate mixtures of SB dissolved in silicate solutions and metakaolin, which reveal geopolymer bodies of significant strength (up to 35 MPa). But such cements could not protect SB from destruction and the whole hydrogen content was lost after about seven days, leaving only destruction products of SB behind.

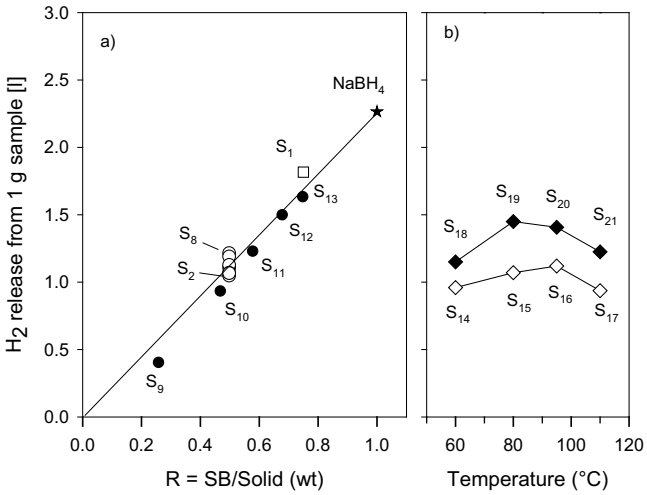

Fig. 6: Hydrogen release in liter gas per g sample a) as a function of R = SB/solid (wt) as used (Table 1) for series of S2-S8, S9 – S13, S2, and of NaBH4 (solid line as guide to the eye), and b) for series S13 – S16 (R = 0.47), S17-S21 (R = 0.57) as a function of the drying temperature.

The numbers given in the last column in Table 1 denote an equivalent amount of SB enclosed in the geopolymer with respect to the amount of hydrogen released by acid titration. Obviously, there is a systematic increase from about 61 % to 85 – 86 % with increasing SB/solid ratio over the series S9 – S13. However, these numbers do not take into account the water content of the geopolymer. In separate investigations, it could be shown that the total water content of the samples is related to the geopolymer [17, 18]. There was a linear decrease in loss related to the water content from about 9 wt% to 4 wt% for a sample of SB/solid = 0.37 to 2, respectively. The data could be extrapolated to no water content for pure SB (i.e. SB/solid = 1). It may be noted, that the water content of the geopolymer varies dependent on the heating (drying) and reloading conditions,

similar to the behavior for zeolites, leading to variations in the absolute values depending on the holding conditions. Compositional and structural variations of the geopolymer network could also influence the hydrogen content. For example, the hydrogen released increases gradually somewhat for samples dried at 110 °C from 1.06 L/g for S2 to about 1.21 L/g for S8, i.e. with increasing Si/Al ratio. The hydrogen released for the series of samples dried at 80 °C behaves in a similar way and supports the results obtained for the 110 °C-dried samples (compare Table 1). It might be interesting to note that the "drying temperature" also influences to an extent the amount of hydrogen available, as investigated in detail in [18]. Dried at 80 °C and 95 °C, SB-G released about 15 % more hydrogen compared to synthesized samples dried at 110 °C and 60 °C (Fig. 6b, series S14 – S17, S18 – S21, Table 1). When temperatures below 60 °C were used, the samples did not dry completely. Samples treated at 40 °C remained wet even after 24 h of drying, without, however, revealing significant amounts of SB destruction products. Similarly, the SB in vacuum-dried samples (at 20 °C) remained stable, showing however systematically lower hydrogen contents relative to the higher water content of the samples [13].

The formation of carbonate was quantified with a carbon-sulfur analysis technique [18]. It ranges between 0.3 wt% for highly enriched SB-G and 3.2 wt% for SB-G containing intermediate amounts of SB. Carbonate forms mainly in the alkaline solution adsorbing CO_2 from the atmosphere during handling. Obviously, the influence of CO_2 can be reduced using higher amounts of SB dissolved in the aluminate and silicate solutions.

The combination of synthesis parameters for an optimized SB content indicates an optimum using SB-saturated aluminate and silicate solutions possessing a Si/Al ratio between 2.5 and 3 and drying temperature between 80 and 90 °C. This was used for preparing sample S1 (Table 1), which shows the highest amount of hydrogen that could be released, 1.8 L/g SB-G.

(d) ***TG/DTA***

Some TG/DTA experiments were conducted on SB-G samples in comparison to pristine SB as shown in Fig. 7 using flowing He or technical air (80/20 N_2/O_2, wt%). Compared to the effect observed in technical air, there is virtually no change in mass up to 400 °C of SB when He is used as inert gas, Fig. 7a. Enlarging the scale makes a decrease in mass of about 1 % (wt) up to 150 °C visible (inset Fig. 7a), which is related to desorption of residual H_2O. Urgnani *et al.* [19] performed a thermal desorption analysis of SB under vacuum coupled to a mass spectrometer. The data showed some desorption of H_2O up to about 150 °C, too. A small but significant release of hydrogen could also be detected, peaking at about 250 °C, 350 °C and 450 °C. The majority of hydrogen was released above 500 °C in two steps, after the sample was molten. A release of hydrogen could also be sensitively detected starting from 200 °C and followed up to 400 °C in temperature-dependent infrared absorption (TIR) experiments using a special nitrate-tracer technique for SB and $NaNO_3$ highly diluted in the KBr pellet [20] by observing the reaction

$$NO_3^- + H_2 \Rightarrow NO_2^- + H_2O \qquad (1)$$

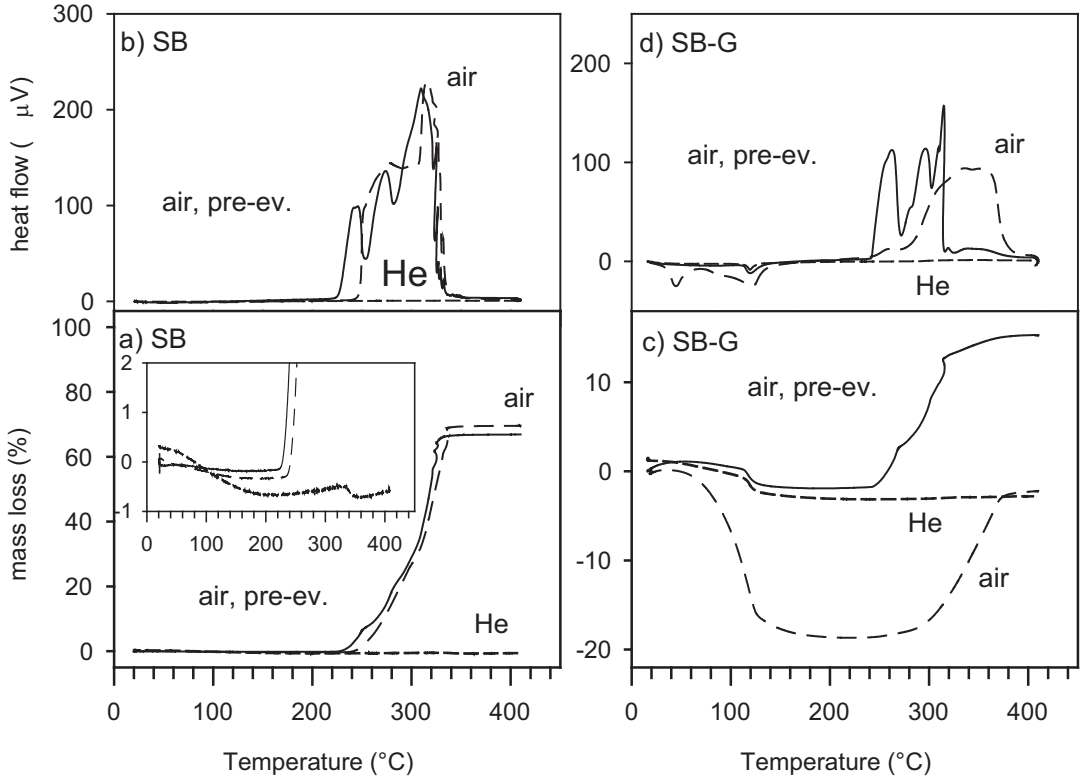

Fig. 7: Mass loss and heat flow of as-received SB (a, b) and SB-G sample, Gel_80_1, (c, d) in TG/DTA experiments using flowing He (dashed line) and technical air conditions. Flowing technical air was used, filling the evacuated sample chamber (to 10^{-5} mbar) up to normal pressure within 15 min, before starting the heating run (air, pre-ev. Solid line), similar to that when using He as inert gas. For the "air"-denoted curves (dot-dashed), it was just switched to technical air with a flow of about 15 min before heating.

It also could be shown that the formed H_2O enforces further hydrogen release together with first indications of polymerized $B_3O_6^{3-}$ rings in the spectra above 300 °C owing to the destruction of SB. Such measurements are carried out with rather spurious contributions of H_2O or O_2 leading to minor effects of destruction of SB and of SB-G [20]. On the other hand, heating in air, i.e. under open conditions, leads to a strong increase in mass with an onset at about 240 °C, reaching almost 69 % in addition to the starting value. For a pre-evacuated sample, a systematic lower onset by about 10 °C is observed, reaching an additional mass of about 67 %. The increase in mass is explained by the reaction

$$NaBH_4 + 2O_2 \Rightarrow NaBO_2 + 2H_2O \qquad (2)$$

The increase in mass almost agrees with the expected value of 73.9 %, indicating a complete destruction of SB with reaction (2) under air flowing conditions distributed over 100 °C. The reaction occurs in three main exothermic steps, which are observed in a quite analogous form for Sb-G under the same conditions as for the pre-evacuated sample (Fig. 7b, d), too. However, the third step shows a much steeper drop, revealing a reduced temperature distribution of the reaction. Additionally, the total increase in mass amounts to only about 15 % (wt) of the initial value (Fig. 7c), which indicates that larger amounts of SB remain unreacted within the SB-G.

Below 220 °C, the mass loss shows almost the same curves under technical air and He flowing conditions owing to the pre-evacuating treatment. Thus, adsorbed water and some amount of water in the pores of the geopolymer network can be desorbed by this treatment, i.e. in total about 18 wt% for the present sample. But the surface of SB crystals inside the SB-G still seems to be strongly modified, or covered, retarding the observed main increase in mass due to reaction (2) by about 50 °C. Similar behavior could also be observed for an SB-G of Si/Al = 2. Further investigations are necessary to fully understand the details of these observations.

(e) ***SEM***

SEM images of the sample S1 are shown in Fig. 8 at different resolutions. Typically, at smaller resolution *75 (Fig. 8a), some agglomerates of particles in sizes of 50 to 100 µm are observed, which seem to be better resolved in magnification *370 (Fig. 8b). These particles are composed of sub-particles of voluminous features with many holes inside, as observed in magnification *5000 (Fig. 8c). EDX analysis always shows Na, Al, Si as signals. There seems to be no uncovered SB-crystals, which could not be observed directly at such low resolution. Their typical size is of the order of 20 – 40 nm as deduced from the XRD using the Scherrer equation.

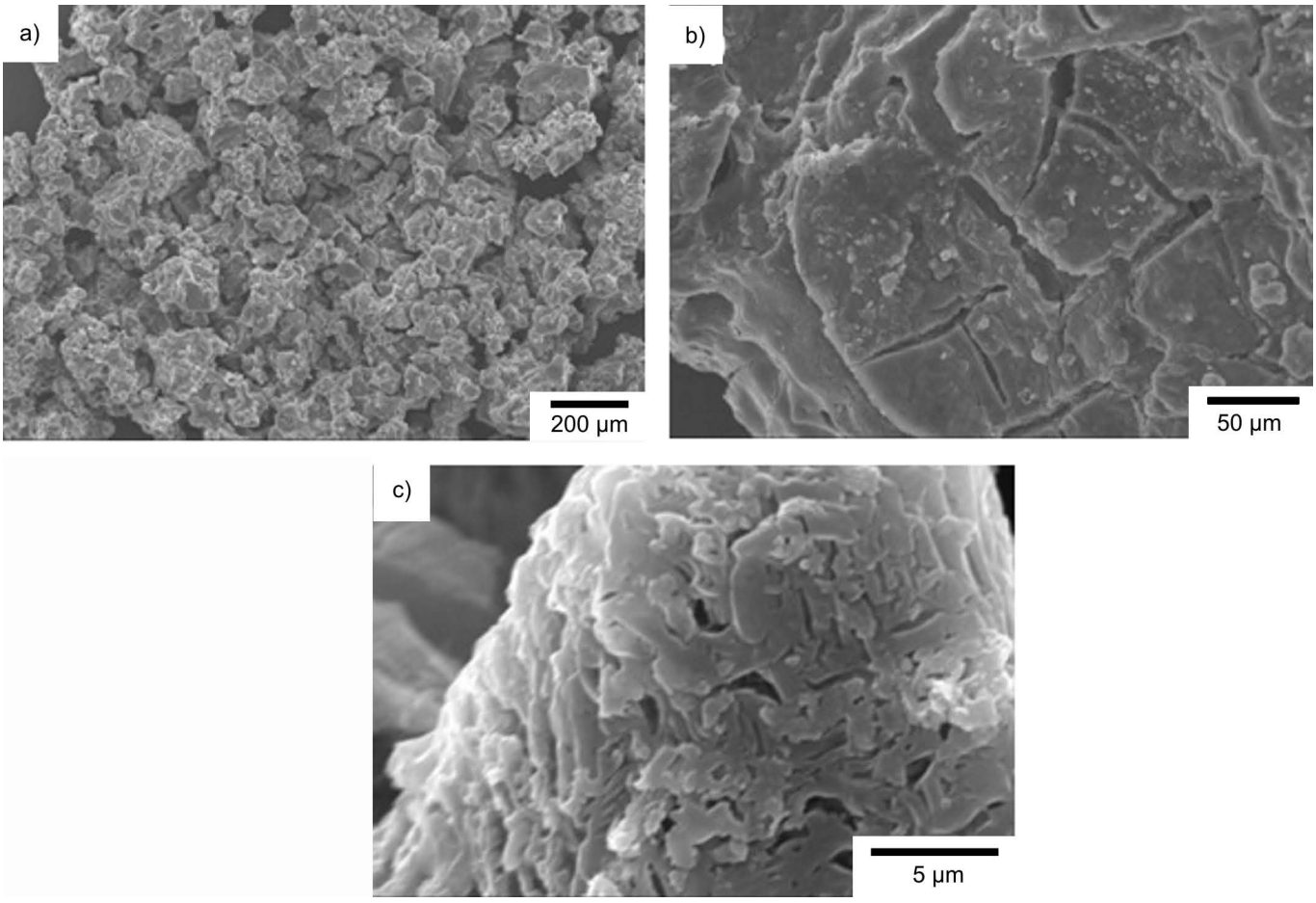

Fig. 8: SEM photographs of the sample S1 (Table 1) at different magnitudes a), b), c) as denoted.

(2) AB-G composites

(a) ***XRD***

The X-ray powder pattern of the as-received AB and the synthesized white powder for one example of AB-G is shown in Fig. 9. AB crystallizes in space group I4mm, a = 5.244 Å, b = 5.033 Å. All main reflections for AB are also seen for AB-G. Some additional reflections of low intensities could indicate some destruction products of AB in AB-G but were not further specified. Other additional peaks could be identified as sodalite phase. The peaks of AB in the AB-G show symmetric profiles whereas the reflections of the as-received AB show largely asymmetric peaks, indicating a significant contribution distributed towards lower diffraction angles, as depicted more clearly in the inset of Fig. 9. The more symmetric form of the peaks indicates more perfect crystals for AB recrystallized in AB-G. The average crystal size of AB in AB-G could be estimated for some selected peaks to be in the range of 40 – 60 nm using the Scherrer equation. Similar average crystal sizes could also be obtained for SB recrystallized in SB-G composites.

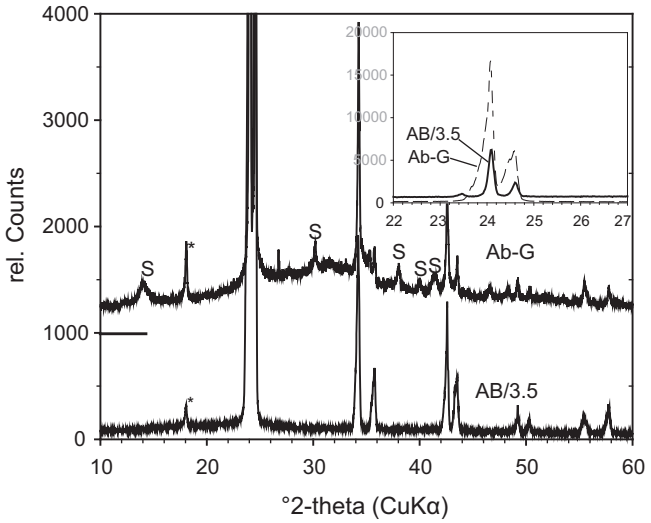

Fig. 9: XRD pattern of AB and AB recrystallized in the geopolymer (AB-G, shifted by 1000, , AB divided by 3.5). Inset zoomed for 22° to 27° 2-theta showing the two strongest peaks). S mark sodalite peaks. Peak * due to sample holder.

In addition to diffraction peaks of AB, the XRD pattern of the AB-G samples showed a broad hump between 20° and 40° 2-theta centered at about 30°-32° 2-theta. This contribution is attributed to the geopolymer formed by the condensation of appropriate units during mixing of the aluminate and silicate solution, similar to the effect in the XRD pattern of SB-G (Fig. 2).

(b) ***IR absorption***

Typical spectra of AB, AB-G and a geopolymer are compared in Fig. 10. A geopolymer as constituted for the 35/65 % (metakaolin/waterglass wt%) aged 4 days is characterized by IR-absorption (KBr-method) by a peak maximum at 1016 cm^{-1} attributed to asymmetric Si-O vibrations of the $[Si\text{-}O_4]^{4-}$ tetrahedral type unit as has been assigned as the DOSPM (density of states peak maximum). The geopolymer spectra closely coincide with those of aluminosilicate glasses, also with regard to the other Si-O-related peaks centered at 780 cm^{-1} and 480 cm^{-1} [21]. The peak at about 700 cm^{-1} is related to the $[AlO_4]^{5-}$ units. The absorption peak at 860 cm^{-1} indicates the presence of significant amounts of Si-OH groups. It has been observed that this peak becomes gradually reduced in intensity with heating between 100 and 600 °C owing to further condensation and dehydration. H_2O-related absorption peaks are observed at 1630 cm^{-1}, 3000 – 3600 cm^{-1}. The absorption peaks in the range 1400 – 1480 cm^{-1} are due to formation of CO_3^{2-} through the reaction of NaOH solution with CO_2 during handling under atmospheric conditions. The peaks of AB in the IR spectrum are assigned to (all in cm^{-1}): 782, 798 B-N stretching; 727, 1064 NBH rocking; 1178, 1162 BH_3 deformation; 1378, 1605 NH_3 deformation; 2280 BH sym. stretch; 2377, 2332 BH asym. stretch; 3250, 3318 N-H asym. stretch. All peaks observed for AB are also seen in Ab-G, showing that AB recrystallized. The IR spectra of AB-G samples also indicate the formation of mainly sialate-type structural units with the peak centered at about 975 cm^{-1}, including also a contribution of the sodalite. The typical triplicate absorption peaks of sodalite may be recognized (compare also Fig. 4 in the range 600 – 700 cm^{-1}). Si-OH groups are indicated by the shoulder at 860 cm^{-1}, as well as indications of carbonate and H_2O related to the matrix.

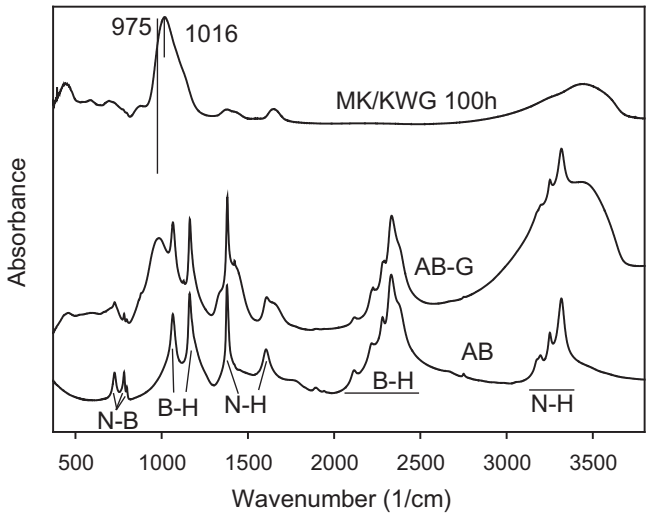

Fig. 10: Infrared absorption spectra of AB, AB-G. A typical spectrum of a geopolymer cement is shown for comparison, too (from metakaolin/waterglass 35/65 %, aged 4 days). N-B, B-H denote peak positions or ranges of vibrations.

(c) ***Hydrogen content and stability checks***

Acid titration could also be used for releasing hydrogen from amino boranes (e.g. [22]). Therefore, we checked the gas evolution in the same way as described above for SB and SB-G samples. In Fig. 11 results are shown as directly obtained with the 100-mL bulb (Fig. 1) for different mass used for AB, AB-G, SB and an optimized SB-G. For the used example of AB-G, the regression analysis reveals 0.71 L hydrogen per g sample used. For comparison, for AB we obtained 1.97 L/g, i.e. the present AB-G sample could contain about 36 % AB effectively included. Ideally

AB contains 19.5 wt% hydrogen per formula unit, i.e. almost twice as much as SB (10.58 wt%). However, only the hydride-anions of the H_3B-part are released in hydrogen by acid titration as described by

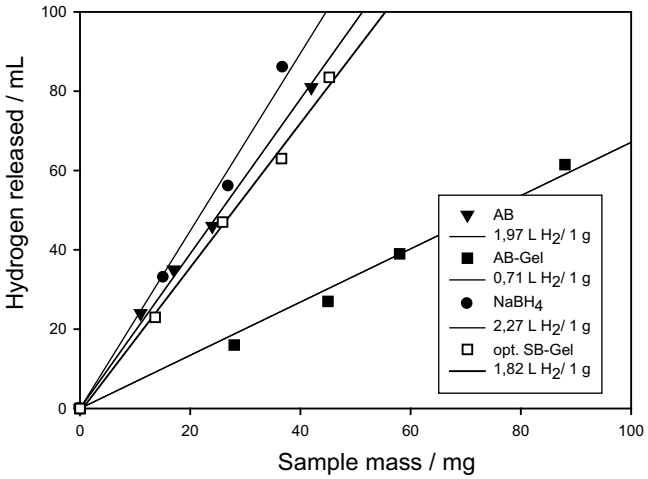

Fig. 11: Experimental determined hydrogen release as a function of used sample mass for AB, AB-G, SB and SB-G (sample S1) with regression lines.

$$\begin{matrix} H_3N\text{-}BH_3 \\ + H^+ + 3H_2O \Rightarrow 3H_2 + B(OH)_3 + NH_4^+ \end{matrix} \quad (3)$$

With the use of hydrochloric acid, the formation of NH_4Cl could be expected, as could be observed in the IR-absorption spectra of the residuals after the titration (Fig. 12). This explains that the hydrogen released by acid titration is slightly less for AB as compared to SB, considering that in both cases half of the hydrogen is attributed to protons of the acid.

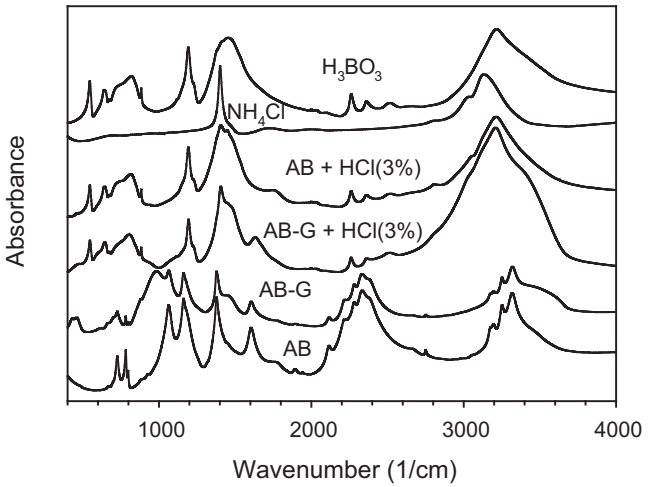

Fig. 12: Infrared absorption spectra of AB, AB-G and filtrates of AB and AB-G after ACHR (acid catalyzed hydrogen release) using 3 % HCl solution. Spectra of NH_4Cl and H_3BO_3 are shown for comparison.

It is also observed in Fig. 12 that the acid titration reveals boric acid as the other main product as given in reaction (3). This is similarly observed also for the solid residuals of the acid-treated AB-G sample. Moreover, the spectra reveal that the geopolymer and also the sodalite completely disappeared. This is clear since any sialate group will be immediately destroyed in acid. The Al^{3+} ions become dissolved as $AlCl_3$, whereas the Si^{4+}-containing units will condense into silica. The silica can be seen in the spectra as an additional shoulder around 1100 cm^{-1}. It may be noted that aging of AB-G samples did not show such long-term stability as for SB-G. For example, indications of $NaB(OH)_4$ destruction product could be observed after about four months, even when the samples were kept in a closed glass bottle in the laboratory. On the other hand, better stability is exhibited by AB-G in water compared to AB. This could be observed given AB and AB-G in neutral water (about 40 mg in 1 mL) and drying of this at 80 °C under open conditions. This reveals some white powder. The IR absorption spectra showed that the AB sample becomes transformed into polyaminoborate species [14] whereas the AB-G sample remains unchanged. The AB-G sample was dried for 3 h at 80 °C after mixing the AB-containing aluminate and silicate solutions. Rehydration of this sample and further handling at 80 °C showed therefore that AB is protected by the geopolymer part matrix at least against reaction with water. Both AB and AB-G remain stable when heated at 80 °C for 20 h. AB and also AB-G were further treated in alkaline solution (50 mg in 1.5 mL 1M NaOH-solution). The filtrates were dried at 80 °C under open conditions, revealing in both cases $NaB(OH)_4$ as destruction products.

(d) ***TG/DTA experiments.***

TG (thermogravimetric), dTG (differential themogravimetric) and DTA (differential themoanalytic) data for the AB and AB-G samples are shown in Fig. 13. No reliable data could be obtained for AB above about 120 °C owing to a strong exothermic reaction related to a loss of sample from the crucible. The AB-G sample reveals a total mass loss of about 11.8 %, including two main steps centered at about 122 °C and 145 °C. These steps are related to a loss of about 5 % and 3 %, respectively. A mass loss due to dehydration of the geopolymer could also be expected and is probably seen starting from about 50 °C. Its total contribution may be estimated to about 2 % – 3 %. Assuming that the loss of 8 % is related to the release of two mole of hydrogen from AB, this implies that about 40 – 50 % of AB has been included in this AB-G sample, a value indicating that almost 90 – 100 % of AB given as an educt was enclosed in AB-G. The heat flow shows a small exothermic effect, followed by some endothermic effect before a strong exothermic peak is observed. The endothermic effect here is related to the melting of AB. This indicates that hydrogen formation starts here at a slightly lower temperature before significant melting occurs. Both effects seem to be closely related to each other, in the AB-G sample as well, as could be realized for the AB sample, too. For the AB-G sample a second exothermic peak is observed with a maximum at about 160 °C. The start of a second strong exothermic effect may also be suggested for the AB curve, which could not, however, be evaluated further owing to the explosive loss of sample as described above. The question arises if both exothermic peaks for the AB-G could be related with hydrogen release and if a mass loss owing to the evaporation of any other gas could be ruled out.

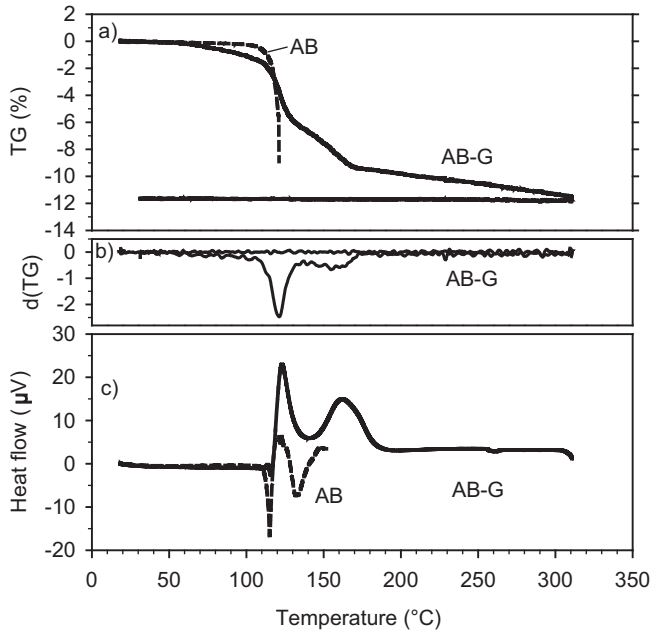

Fig. 13: Results of thermogravimetric analysis (TG), a.) and differential thermo analysis (DTA) c.) of AB-G (solid line) and AB (dashed).

Frueh *et al.* [23] and Fang *et al.* [24] reported two exothermic peaks for AB at the same temperature observed here for AB-G. Both author groups used the same heating rates of 5 K/min, either under flowing argon or nitrogen. Frueh *et al.* obtained between 110 and 130 °C a mass loss of about 20 %, followed by a loss of about 30 – 34 % in a second step between 140 and 160 °C. These authors could analyze parallel to the TG-measurement two maxima in hydrogen release, at 120 °C and at 155 °C by means of mass spectrometry. Similar results were also obtained by Zhang *et al.* [4]. Since a total mass loss related to hydrogen could only be 19.6 %, there was a loss in N and B. A degassing of borazine could be detected by Zhang *et al.* [4] and also by Fang *et al.* [24] above about 160 °C. Zhang *et al.* [4] reported that hydrogen was mainly released, peaking at about 120 °C and 150 °C, and borazine at 160 °C in pristine AB. For AB infiltrated in silica hollow nanospheres (SHNS), the hydrogen release curve could be shifted to a lower temperature (up to 30 °C). Degassing of borazine also becomes somehow reduced and shifted to a lower temperature or even disappears below the detection limit, too. Similar results were reported by Gutowska *et al.* [3] for AB infiltrated in SBA-15.

For a further investigation of the mass loss effects, we concentrated in a first step on the destruction products, which could be observed in the solid residuals. Parts of the sample were heated in a furnace under open conditions with heating rates 5 K/min to 120 °C, 150 °C and 300 °C. Samples were taken out of the furnace immediately when they reached the temperature and were also checked after certain holding times (5 min, 10 min, 15 min). The samples were pressed into KBr pellets immediately after they had been taken out of the furnace and the IR-absorption was measured. Selected spectra are shown in Fig. 14. As seen above, AB melts at 118 °C with foaming. When the melt of AB was pressed in KBr pellets, the spectra showed a remarkably high intensity of all main AB peaks compared to as-received AB (Fig. 14a). Additionally, peaks indicating the formation of $[BH_4^-]$-groups were observed. The $[BH_4^-]$-related peaks were absent in the IR spectrum of the soft white powder produced when this was heated slightly longer at 120 °C (5 min). AB disappeared, too. Instead IR absorption of poly-aminoboranes (PAB) were observed. This could be described by an effective reaction

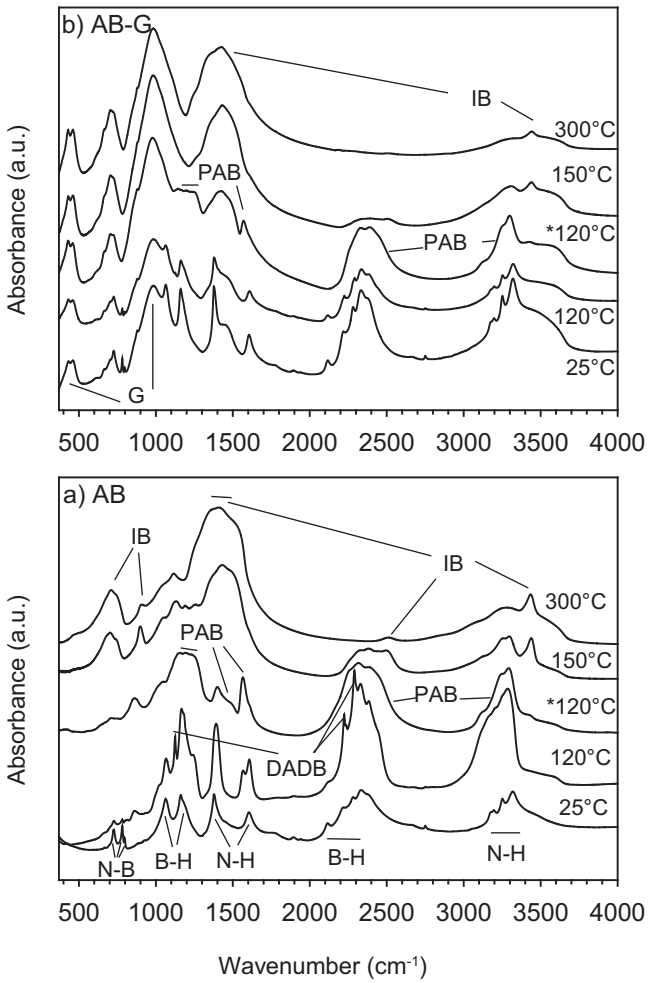

Fig. 14: Infrared absorption spectra of AB (a) and of AB-G (b) samples heated in a furnace under open conditions. *120 °C denotes a sample heated for 5 min (further details are in the text).

$$H_3N\text{-}BH_3 \Rightarrow H_2 + 1/n\ (\text{-}H_2N\text{-}BH_2\text{-})_n \qquad (4)$$

For example, for n = 1, $H_2N{=}BH_2$ could be evaporated from the melt. Instead, polymerization reactions could reveal more stable PAB $(\text{-}H_2N\text{-}BH_2\text{-})_n$ [23], including a linear dimer of aminoborane (LDAB) as a transition state [25]:

$$2H_3N\text{-}BH_3 \Rightarrow H_2 + NH_3BH_2NH_2BH_3 \qquad (5)$$

$$NH_3BH_2NH_2BH_3 \Rightarrow H_2 + 1/n\ (\text{-}H_2N\text{-}BH_2\text{-})_n \qquad (6)$$

In further heating experiments at 120 °C (10 min, 20 min), it was observed that the PAB-related peaks already decreased in intensity and some signature of PIB (polyiminoboranes) appeared. A mixture of PAB and PIB is also observed for heating at 150 °C (Fig. 14a, spectrum taken after 10 min). The spectrum observed after heating at 300 °C reveals just the presence of PIB. The transforma-

tion of PAB into polyiminoboranes (PIB) can be described by:

$$1/n\ (\text{-}H_2N\text{-}BH_2\text{-})_n \Rightarrow H_2 + 1/n\ (\text{-}HN{=}BH\text{-})_n \qquad (7)$$

which is related to the release of hydrogen in a second step, but may be realized already at 120 °C, too. The *ex-situ* results obtained for the AB-G sample showed quite analogous behavior, without, however, a signature of $[BH_4^-]$-groups in the series of experiments shown in Fig. 14b.

Weak indications of $[BH_4^-]$-groups could also be observed for AB-G in some preliminary spectra [14]. The formation of larger amounts of $[BH_4^-]$-groups occurs during melting of AB and pressing into the KBr pellet. This could be realized in (*in-situ*) TIR experiments for AB and AB-G, too [20]. Thereby the KBr matrix obviously enables an ion exchange between the Br- of the KBr and $[BH_4^-]$-groups in the AB-melt, thus forming a $K(BH)_4$-KBr solid solution. A similar effect was not observed for AB and AB-G pressed in NaCl in TIR experiments, which could be explained by the different ion radii of Cl^- and $[BH_4]^-$ and the similar sizes of $[BH_4]^-$ and Br^- [26]. This implies that the coverage of the geopolymer might not be very thick or cannot significantly stop the ion migration.

The formation of $[BH_4^-]$- groups indicates some hydride transfer to "upgrade" [-BH3]-groups which could be described by

$$2H_3N\text{-}BH_3 \Rightarrow [(NH_3)_2BH_2]BH_4 \qquad (8)$$

with the formation of di-ammoniate of diborane (DADB) without any hydrogen release [23]. On the other hand, Stowe *et al.* [27] suggested the formation of DADB as an intermediate step towards formation of PAB, based on ^{11}B MAS NMR investigations, via:

$$[NH_3\text{-}BH_2\text{-}NH_3]^+[BH_4]^- + AB \Rightarrow [NH_3\text{-}BH_2\text{-}NH_2\text{-}BH_2\text{-}NH_3]^+[BH_4]^- + H_2, \text{ etc.} \qquad (9)$$

According to Stowe *et al.* [27], DADB behaves like an activated form of AB, where the cationic part enforces the further reaction into PAB, attributing one protonic hydrogen and hydridic hydrogen from the $-NH_3$ and $-BH_3$ parts, respectively, with $[BH_4]^-$ used for charge neutrality. Bowden *et al.* [28] confirmed the formation of an activated phase [AB]* and DADB prior to the release of the first mol of H_2. The capture of the $[BH_4^-]$-ion in the KBr matrix could support such an explanation.

(e) ***SEM***

Fig. 15 shows typical SEM images for AB-G (a) and AB (b) with a magnification of *4000 and *370, respectively. The higher magnification was necessary for the AB-G samples since the typical particle size was much finer compared to that of the AB as-received sample. This could be related to the solution recrystallization process of the crystals. For the AB sample, only B and N were obtained with EDX analysis whereas for AB-G very strong signals for Si, Al, and Na were seen compared to some weak identifications of B and N. This shows that AB crystals are well covered by the geopolymer.

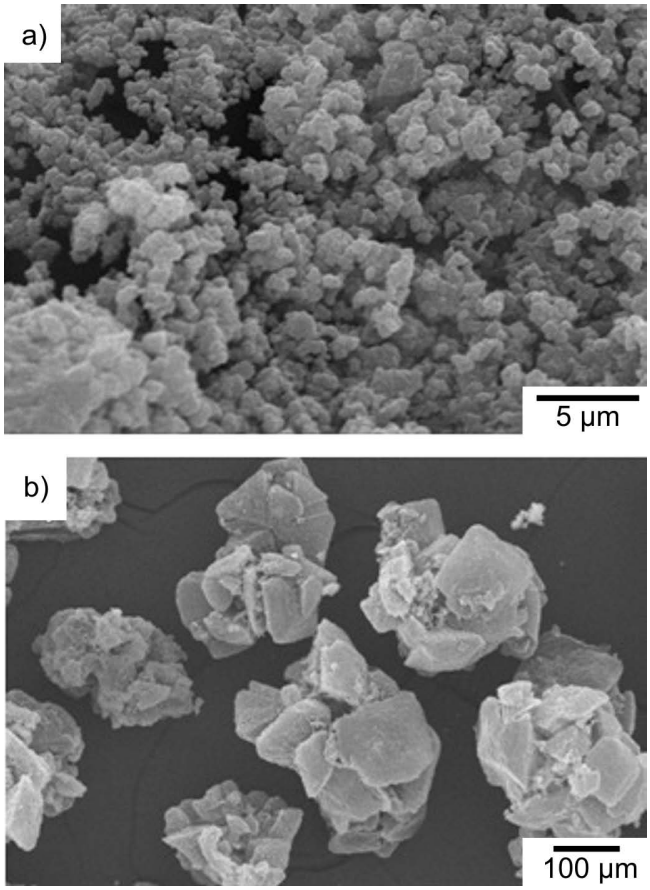

Fig. 15: SEM photographs of a) AB-G and b) AB. (Modified from [14]).

IV. Conclusions

The new $NaBH_4$- and NH_3BH_3-geopolymer composite may offer interesting properties as an alternative to the use of other hydride-scaffold scenarios like AB infiltrated into SBA-15, MCM-41, or silica hollow nanospheres. The handling might be rather simple, i.e. using open conditions and dissolution in aluminate and silicate solutions. Further optimization procedures for AB-composites might be considered, following those carried out for the SB-geopolymer composites: e.g. variations in the Si/Al ratio of the geopolymer, in the solid/solution ratio determining the degree of solubility of AB in silicate and aluminate solution and considering variations in drying procedures. Interesting open questions concern details of thermolysis, particularly if the hydrogen-releasing temperature could be lowered using a Si-rich geopolymer scaffold similar to SBA-15 or silica hollow nanospheres. Future work could include developments of some catalyst techniques with regard to the thermal hydrogen release from AB-G and SB-G.

Acknowledgements

Part of the work was supported by DFG under RU 764/6 – 1.

References

1 Tang, Z., Chen, X., Chen, H., Wu, L., Yu, X.: Metal-free catalysis of ammonia-borane dehydrogenation/regeneration for a highly efficient and facilely recyclable hydrogen storage material, *Angew. Chem. Int. Ed.*, **52**, 5832 – 5835, (2013).

[2] Gutowska, A., Li, L., Shin, Y., Wang, C.M., Li, X.S., Linehan, J.C., Smith, R.S., Kay, B.D., Schmid, B., Shaw, W., Gutowski, M., Autrey, T.: Nanoscaffold mediates hydrogen release and the reactivity of ammonia borane, *Angew. Chem. Int. Ed.*, **44**, 3378 – 3582, (2005).

[3] Zhang, T., Yang, X., Yang, S., Li, D., Cheng, F., Tao, Z., Chen, J.: Silica hollow nanospheres as new nanoscaffold materials to enhance hydrogen releasing from ammonia borane, *Phys. Chem. Chem. Phys.*, **13**, 18592 – 18599, (2011).

[4] Li, P.-Z., Aranishi, K., Xu, Q.: Zif-8 immobilized nickel nanoparticles: Highly effective catalysts for hydrogen generation from hydrolysis of ammonia borane, *Chem. Commun.*, **48**, 3173 – 3175, (2012).

[5] Nielsen, T.K., Karkamkar, A., Bowden, M., Besenbacher, F., Jensen, T.R., Autrey, T.: Methods to stabilize and destabilize ammonium borohydride, *Dalton T.*, **42**, 680 – 687, (2013).

[6] Barrer, R.M.: Hydrothermal chemistry of zeolites. London Academic Press, 384 (1982).

[7] Buhl, J.C., Gesing, T., Rüscher, C.H.: Synthesis, crystal structure and thermal stability of tetrahydroborate sodalite $Na_8[AlSiO_4]_6(BH_4)_2$, *Micropor. Mesopor. Mat.*, **80**, 57 – 63, (2005).

[8] Buhl, J.C., Gesing, T., Höfs, T., Rüscher, C.H.: Synthesis and crystal structure of gallosilicate- and aluminogermanate tetrahydroborate sodalites $Na_8[GaSiO_4]_6(BH_4)_2$ and $Na_8[AlGeO_4]_6(BH_4)_2$, *J. Solid State Chem.*, **179**, 3877 – 3882, (2006).

[9] Buhl, J.C., Schomborg, L., Rüscher, C.H.: Tetrahydroborate sodalite nanocrystals: low temperature synthesis and thermally controlled intra-cage reactions for hydrogen release of nano- and micro-crystals, *Micropor. Mesopor. Mat.*, **132**, 210 – 218, (2010).

[10] Buhl, J.C., Schomborg, L., Rüscher, C.H.: Enclosure of sodium tetrabydroborate ($NaBH_4$) in solidified aluminosilicate gels and microporous crystalline solids for fuel processing, in Hydrogen Storage, J. Liu ed., INTECH ISBN 978 – 953 – 51 – 0371 – 6, free online editons, Chapter 3, 49 – 90, (2012).

[11] Rüscher, C.H., Schomborg, L., Schulz, A., Buhl, J.C.: Basic research on geopolymer gels for production of green binders and hydrogen storage. In: Developments in strategic materials and computational design IV, ed. by W.M. Kriven, J. Wang, Y. Zhou, A.L. Gyekenyesi, *Ceram. Eng. Sci. Proc.*, **34**, [10], 97 – 114, (2013).

[12] Ponce de Leon, C., Walsh, F.C., Pletcher, D., Browning, D.J., Lakeman, J.B.: Review: direct borohydride fuel cells, *J. Power Sources*, **155**, 172 – 181, (2006). Compare also Z. P. Li, B. H. Liu, K. Arai, K. Asaba, S. Suda. Evaluation of alkaline borohydride solutions as the fuel for fuel cell, *J. Power Sources*, **126**, 24 – 33, (2004).

[13] Schomborg, L., Rüscher, C.H., Buhl, J.C., Kiesel, F.: $NaBH_4$ geopolymer composites. In: Developments in strategic materials and computational design V, ed. by W.M. Kriven, D. Zhu, K.I. Moon, T. Hwang, J. Wang, C. Lewinsohn, Y. Zhou, *Ceram. Eng. Sci. Proc.*, **35**, [8], 3 – 14, (2014).

[14] Schomborg, L., Assi, Z., Buhl, J.C., Rüscher, C.H., Wark, M.: Ammonia-borane geopolymer (AB-G) composite. In: Developments in strategic materials and computational design VI, ed. by W.M. Kriven, J. Wang, D. Zhou, T. Fischer, *Ceram. Eng. Sci. Proc.*, **36**, [8], 21 – 35, (2015).

[15] Filinchuk, Y., Hagemann, H.: Structure and properties of $NaBH_4{*}2H_2O$ and $NaBH_4$, *Eur. J. Inorg. Chem.*, 3127 – 3133, (2008).

[16] Rüscher, C.H., Salman, N., Buhl, J.C., Lutz, W.: Letter to the Editor: relation between growth-size and chemical composition of X and Y, *Micropor. Mesop. Mat.*, **92**, 309 – 311, (2006).

[17] Rüscher, C.H., Schomborg, L., Assi, Z., Buhl, J.C.: NH_3BH_3 and $NaBH_4$ enclosed in geopolymers and zeolites. In Ceramics for environmental sytems, ed. by L. Wang, N. Imanaka, W.M. Kriven, M. Fukushima, G. Kale, *Ceram. Trans.*, **257**, 105 – 118, (2015).

[18] Schomborg, L.: Aluminosilicate borohydrides: $NaBH_4$ embedded in sodalite and gel structures. Diss.University of Hannover. Leibniz Information Centre for Science and Technology University Library Catalogue (LUH, TIBKAT), 1 – 204, (2015).

[19] Urgnani, J., Torres, F.J., Palumbo, M., Baricco, M.: Hydrogen release from solid state $NaBH_4$, *Int. J. Hydrogen Energ.*, **33**, 3111 – 3115, (2008).

[20] Assi, Z., Schomborg, L., C. H. Rüscher, C.H.: Investigations of the thermally induced hydrogen release of $NaBH_4$, NH_3BH_3 and their geopolymer composites. In Development in Strategic Ceramic Materials II: A collection of papers presented on the 40th international conference on advanced ceramics and composites. Ed. by W.M. Kriven. J. Wang, Y. Zhou, D. Zhu, G.K. Costa, **37**, [7], 93 – 108, (2016).

[21] Rüscher, C.H., Mielcarek, E.M., Wongpa, J., Jaturapitakkul, C., Jirasit, F., Lohaus, L.: Silicate-, aluminosilicate and calciumsilicate gels for building materials: chemical and mechanical properties during ageing, *Eur. J. Mineral.*, **23**, 111 – 124, (2011).

[22] Hamilton, C.W., Baker, R.T., Staubitz, A., Manners, I.: B-N compounds for chemical hydrogen storage, *Chem. Soc. Rev.*, **38**, 279 – 293, (2009).

[23] Frueh, S., Kellet, R., Mallery, C., Molter, T., Willis, W.S., King'ondu, C., Suib, S.L.: Pyrolytic decomposition of ammonia borane to boron nitride, *Inorg. Chem.*, **50**, 783 – 792, (2011).

[24] Fang, Z., Luo, J., Kang, X., Xia, H., Wang, S., Wen, W., Zhou, X., Wang, P.: Facile solid-phase synthesis of the diammoniate of diborane and its thermal decomposition behavior, *Phys. Chem. Chem. Phys.*, **13**, 7508 – 7513, (2011).

[25] Zhang, J., Zhao, Y., Akins, D.L., Lee, J.W.: Thermal decomposition and spectroscopic studies of preheated ammonia borane, *J. Phys. Chem.*, **C 114**, 19529 – 19534, (2010).

[26] Assi, Z.: Structural and chemical investigations of the thermal behavior of B-H based materials ($NaBH_4$ and NH_3BH_3) and their oxidation metaborate by-products. Diss. University of Hannover. Leibniz Information Centre for Science and Technology University Library Catalogue (LUH, TIBKAT), 1 – 201, (2016).

[27] Stowe, A.C., Shaw, W.J., Linehan, J.C., Schmid, B., Autrey, T.: In-situ solid state ^{11}B MAS NMR studies of the thermal decomposition of ammonia borane: Mechanistic studies of the hydrogen release pathways from a solid state hydrogen storage material, *Phys. Chem. Chem. Phys.*, **9**, 1831 – 1836, (2007).

[28] Bowden, M., Autrey, T., Brown, I., Ryan, M.: The thermal decomposition of ammonia borane: A potential hydrogen storage material, *Curr. Appl. Phys.*, **8**, 498 – 500, (2008).